SERBIAN JOURNAL OF ELECTRICAL ENGINEERING
Vol. 20, No. 2, June 2023, 243-268
UDC: 621.354:621.316.722.1]:004.42MATLAB DOI: https://doi.org/10.2298/SJEE2302243R

Energy Management and DC Bus Voltage Stabilization in a HRES Based DC Microgrid Using HESS

Amit Kumar Rajput[1], Jagdeep Singh Lather[1]

Abstract: This paper proposes a control strategy with stability analysis for a hybrid energy storage system (HESS) in a DC microgrid (DCMG) consisting of hybrid renewable energy sources (HRESs). The proposed control strategy effectively regulates DC bus voltage (DBV), maintains a balance in demand-generation and improves the power quality by flattening the intermittency in PV generation. The proposed configuration harnesses the advantage of both battery energy storage system (BESS) and supercapacitor (SC) energy storage system (SCESS) in the HESS through their effective utilization as per their power and energy densities. A filtration-based control (FBC) has been proposed using PI controllers to generate the reference signals as per inherent internal characteristics of BESS and SCESS. The efficacy of the proposed configuration is analyzed through simulations using Simscape™ module of MATLAB® software. The results are further validated using the FPGA-based real-time simulator Opal-RT.

Index Terms: Battery, Energy management, Fuel cell, Photovoltaic cell, Supercapacitor, Voltage stabilization.

1 Introduction

Microgrids fed through renewable energy resources (RERs) like PV, wind, and fuel cells (FC) have proven to cater to remote areas where conventional grid connectivity may not be feasible. Further, these are economical, eco-friendly, efficient, and have low maintenance and running costs. These microgrids are categorized into AC, DC or hybrid AC-DC based on the nature of bus and load interconnections. These microgrids are categorized into AC, DC, or hybrid AC-DC. Currently, DCMGs are more intriguing than their AC or hybrid AC-DC counterparts for electricity supply in residential and small-scale commercial applications [1]. This is because of their better controllability and higher efficiency due to the reduced number of conversion stages.

[1]Department of Electrical Engineering, National Institute of Technology, Kurukshetra, India;
Emails: gowidrajput@gmail.com; jslather@nitkkr.ac.in

DC appliances have an extra edge in DCMGs over their AC counterparts for their reduced power rating [2]. However, DCMGs require control of DBV and effective power management strategy (PMS) among its various components. Fig. 1 shows a typical DCMG consisting of PV, wind turbine as RERs, battery, and SC as energy storage devices (ESDs) along with control and power management block.

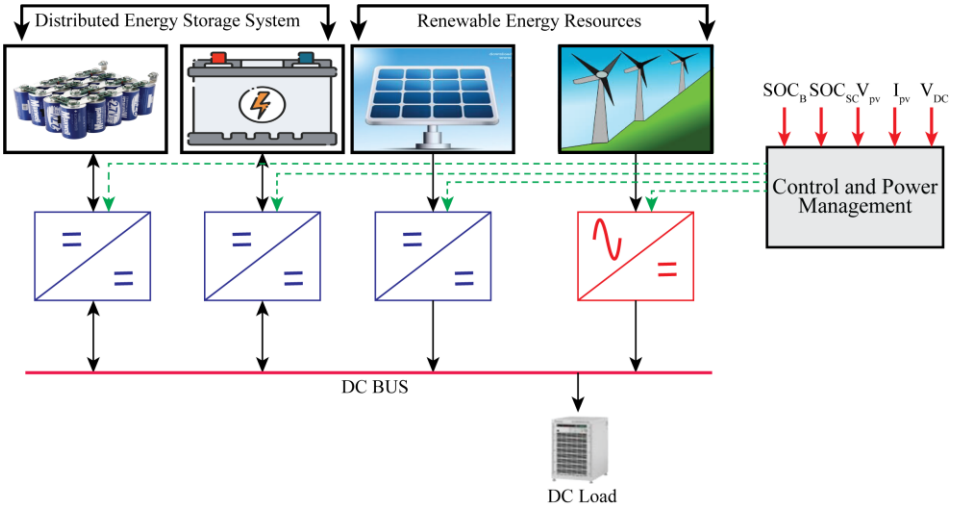

Fig. 1 – *Typical layout of standalone DCMG.*

Electricity generation from RERs (e.g., wind and PV) is intermittent as it relies on atmospheric conditions. Therefore, microgrids consisting of PV and wind power incorporate ESDs to flatten intermittency in PV and wind power generation. This also improves the overall power quality and microgrid stability [3, 4]. A BESS was proposed to support RERs-based microgrid operations under highly fluctuating conditions [5]. A unified PMS was proposed for a hybrid MG incorporating PV-BESS for both on-grid and off-grid modes [6]. However, the stress on BESS and its life cycle was not discussed in the event of irregularity in PV generation. Batteries being high energy density devices, can meet average load demands for a longer period. However, they are unable to address sudden power demands due to their low power density. In contrast, SCs being high-power devices, are better suited to respond during sudden fluctuations in demand-generation. They were used to mitigate randomness in a standalone photovoltaic-BESS-based microgrid [7]. However, SCs are low energy density devices, which renders them unfit to sustain high power demand for extended durations. Fig. 2 represents the various ESDs along with their energy and power densities.

Fig. 2 shows that SC has high-power and low-energy densities, whereas battery has high-energy and low-power densities. Following this, several researchers have recommended a combination of battery and SC, creating a

HESS, which enhances the system performance and reliability [8, 9]. Fig. 3 shows the various topologies for HESS incorporating a battery and a SC [9], wherein the one shown in Fig. 3a is the simplest and most cost-effective. However, it admits no control over battery and SC, as the power distribution depends only on their internal resistances. The topologies shown in Figs. 3b and 3c only provide active control over one device, resulting in voltage oversizing. Fig. 3d offers advantages over others for its independent control over both ESDs, thus considered in this work.

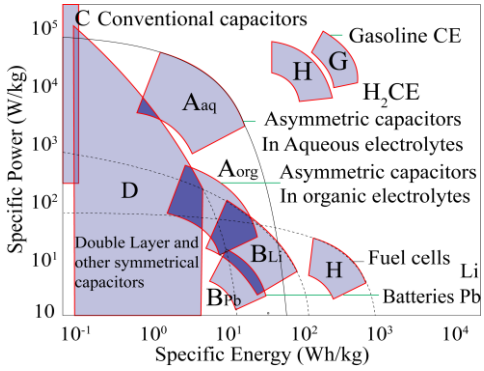

Fig. 2 – *Ragone plot for various energy storage devices.*

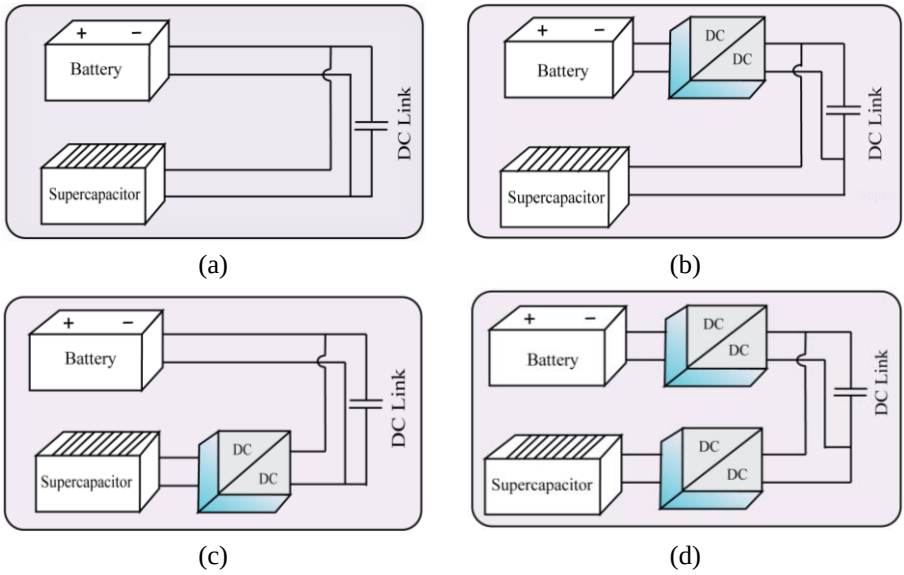

Fig. 3 – *Various topologies for HESS.*

Batteries are employed to ensure constant power supply even in the event of intermittent supply from PV due to bad weather conditions. However, batteries

are unable to store energy beyond a specified range due to technological and device capacity barriers. Therefore, ESDs alone cannot cater during inclement weather conditions and, thus, demand additional power resources to avoid blackouts or power shortages. FCs powered by hydrogen provide an alternate and viable solution to cater continuous power supply to the critical loads under such conditions. They have gained popularity due to their inherent advantages in terms of high efficiency, modularity, and non-polluting nature [10, 11]. The Ragone plot in Fig. 2 ascertains FCs as high energy density devices. In [12], FCs were utilized to mitigate inconsistencies occurring due to intermittent wind power generation. A hybrid microgrid using PV, FC and battery was proposed and implemented to address intermittency in load demands [13]. However, the strategy could not fulfil the fast-changing energy demands, resulting in increased stress on the battery and lowering its effective life. Dong et al. [14] proposed a control strategy for voltage regulation of AC/DC bus in an AC/DC hybrid microgrid. However, the issue of battery overcharging and deep-discharging was not addressed. Furthermore, in [15] they presented a composite converter to connect the BESS and SCESS to MG consisting of PV and wind as DERs. However, bus voltage regulation is not addressed under power discrepancy. Hoang et al. [16] proposed an accurate power sharing in a DCMG incorporating BESS. In their work, batteries could not cope with fast varying loads, putting more stress on BESS and thus reducing battery life. Feng et al. proposed in [17] a multimode fuzzy power allocator for a PV-based MG utilizing battery and SC. However, DBV regulation was not considered. In [18], Hredzak et al. suggested a MPC-based control for segregating low and fast varying power components between BESS and SCESS while maintaining respective SOCs within safe operating boundaries. However, the proposed controller requires complex mathematics and high computational power. In [19], Akar et al. proposed an energy management strategy (EMS) for an EV incorporating battery and SC as composite ESS. The proposed Fuzzy logic control (FLC) based-scheme maintains SOCs under the healthy limits and smoothens battery power profile, however, designing an FLC controller may require domain expertise. Ahmed et al. [20] proposed an EMS for a standalone microgrid configuration consisting of PV/FC/battery and SC. Maximum power is extracted from the PV array utilizing MPPT algorithm. In the proposed EMS, SC has no active role of participation as it is directly connected to DC bus, as shown in Fig. 3b and the battery is not utilized efficiently as the battery SOC is restricted between 56-65.4%. On the other hand, regulation of DBV is not highlighted.

Most of the proposed strategies have employed HESS utilizing battery for slow power mismatch and SC for fast varying power mismatch. HESS has been a subject of interest as it integrates ESDs having complementary characteristics and harnesses the bests of each. Despite their advantages, the existing control

strategies are unable to either effectively regulate DBV or share power among HESS devices or maintain battery SOC in the safe operating zone.

This work proposes an EMS for a DCMG consisting of PV, FC, HESS and a unified controller for DBV voltage regulation, along with its stability analysis and verification of the results through simulation study with validation on HIL platform. The insights presented in this paper are:

- An EMS is proposed to share power effectively between BESS and SCSS in a way to address slow variation in generation or load demand through battery while employing a SC for swift changes in demand-generation.
- Effective regulation of DBV in the face off uncertainty in PV generation and sudden variations in load via proposed stabilizing controller designed for good transient response.
- Maintaining SOCs of battery and SC within boundaries to prevent overcharge or deep discharge to improve their lifetime. Here, SOCs of battery and SC are maintained within $0.2 < SOC_B < 0.8$ and $0 < SOC_{SC} < 1$, respectively.
- Furthermore, the effectiveness of the controller is validated in real-time using OPAL-RT and hardware in loop (HIL) under various operating situations.

This paper is structured as follows: Section 2 presents detailed system configuration and modelling of microgrid components. The proposed control strategy for HESS is discussed in Section 3, while Section 4 deals with controller design for DBV regulation under HESS. Simulation findings in MATLAB/ Simulink and their validation in OPAL-RT are described in Section 5, while Section 6 discusses the conclusion based on the study.

2 System Configuration and Modelling

The considered DCMG configuration includes a PV system, FC generator and HESS comprising of BESS and SCESS. PV and FC are interlinked to DC bus via DC/DC boost converters, whereas bidirectional DC-DC converters (BDCs) connect BESS and SCESS to DC bus, as shown in Fig. 4. Duty cycle for boost converter interlinking PV system and DC bus is estimated using a mode controller. The mode controller acts in MPPT or power control mode (PCM) according to the SOC of battery. When battery SOC is less than 0.8, the MPPT controller generates the duty cycle for boost converter interlinking PV and DC bus; otherwise, the duty cycle is calculated using the PI controller by comparing the reference DBV to the actual DBV.

FC and BESS serve as a backup in a scenario when the PV generation is insufficient to meet load requirements and thereby assist in maintaining DBV at the desired level. However, FC and BESS are not an ideal match for mitigating

demand-generation disparity in fast transient situations. SCESS play a critical role in catering power during fast transient but is unable to provide energy demand for a longer period due to its low energy density.

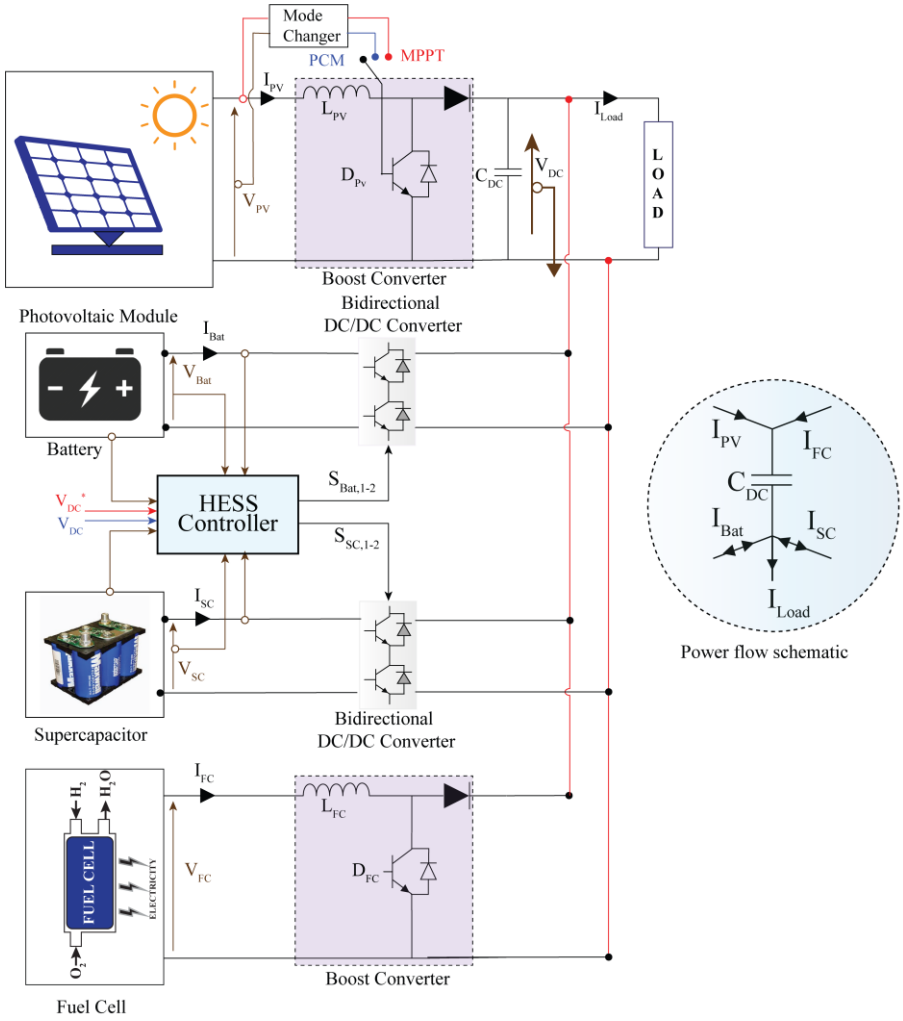

Fig. 4 – *Configuration of the proposed DCMG.*

2.1 PV panel modelling

A solar cell is an elementary unit, which transforms photovoltaic energy into electrical energy. A specified number of solar cells are laid down in series and parallel configurations to produce the desired power output. One diode model of PV cell is utilized in the proposed work. Shunt resistor R_p represents leakage

current and series resistance R_s is internal resistance. The PV current for Fig. 5a is given by

$$I = I_{PV} - I_D - I_p, \tag{1}$$

where I_{PV} stands for photocurrent or direct current generated by sun light, I_D stands for diode current, and I_p represents current in shunt resistor.

Current I_D from the Shockley equation can be written as

$$I_D = I_0\left[\exp\left(\frac{V + IR_s}{nV_t}\right) - 1\right] \tag{2}$$

here, I_0 stands for reverse saturation current and V_t is thermal voltage, V_t is further expressed as

$$V_t = \frac{kT}{q}V, \tag{3}$$

where *k*, *T* and *q* stands for Boltzmann constant, absolute temperature and elementary charge of electron, respectively.

From Ohm's law I_p can be written as

$$I_p = \frac{V + IR_s}{R_p}. \tag{4}$$

From (1), (2) and (4) it follows

$$I = I_{PV} - I_0\left[\exp\left(\frac{V + IR_s}{nV_t}\right) - 1\right] - \frac{V + IR_s}{R_p}. \tag{5}$$

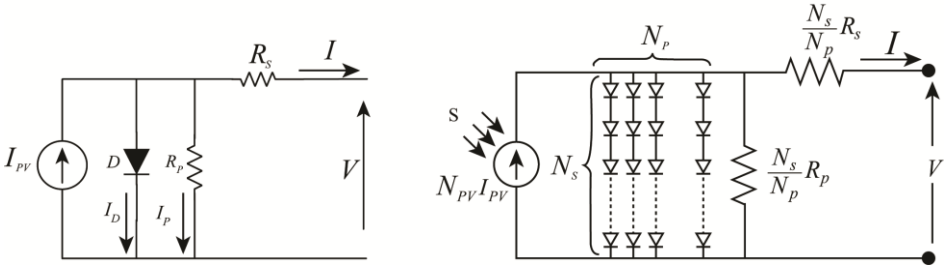

(a) (b)

Fig. 5 – (a) *Equivalent circuit diagram of single diode PV cell;* (b) *PV module.*

PV cells are connected in parallel-series configuration as output from one cell is very low typically 2W. Fig. 5b shows equivalent circuit diagram for one module. Total current of PV can be written as

$$I = N_p I_{PV} - N_p I_0 \left[\exp\left(\frac{V/N_s + IR_s/N_p}{nV_t} \right) - 1 \right] - \frac{V N_p/N_s + IR_s}{R_p} . \quad (6)$$

2.2 FC modelling

A FC is an electrochemical cell that generates electrical energy via a redox reaction that occurs within the cell. FC is an environmentally beneficial option for covering energy shortfalls, and it can be operated indefinitely, if supplied with pure hydrogen and oxygen. The Terminal voltage of FC (V_{FC}) can be expressed as

$$V_{FC} = E_{FC} - V_C - V_{ohm} . \quad (7)$$

Nernst voltage (E_{FC}) can be written as [21]

$$E_{FC} = N_0 \left[E_0 + \frac{RT}{2F} \log \left[\frac{\rho_{H_2} \rho_{O_2}^{0.5}}{\rho_{H_2O}} \right] \right], \quad (8)$$

where: V_C is developed voltage due to FC internal capacitance; V_{ohm} represents ohmic losses of FC; N_0 stands for number of series connected FCs; E_0 is open circuit voltage of FC; R is universal gas constant; T is temperature; ρ_{H_2}, ρ_{O_2} and ρ_{H_2O} represents partial pressure of hydrogen, oxygen and water.

2.3 Mathematical modelling of battery

Batteries are electro-chemical devices that are the most commonly used ESDs in HRES nowadays because of their advancement and widespread availability. Various kinds of electro-chemical battery technologies available (e.g., Lead-acid, Li-ion, NaS, Ni-Cd, Ni-MH), out of which Li-ion battery became the obvious choice for the present work owing to its long life cycle, high energy desity, longevity and low maintenance. The mathematical model of battery is shown schematically in Fig. 6. The Terminal voltage (V_{Bat}) of battery can be written as

$$V_{Bat} = E_0 - K \frac{Q}{Q - \int i \, \mathrm{d}t} + A \exp(-B \int i \, \mathrm{d}t) - R_b i . \quad (9)$$

SOC of battery can be calculated as:

$$SOC_B = 100 \left(1 - \frac{\int_0^t i(t) \, \mathrm{d}t}{Q} \right), \quad (10)$$

where E_0 is constant voltage; K is polarisation voltage (in V); Q represents the maximum ampere-hour capacity; A is exponential voltage of battery (in V); B is exponential capacity (in Ah^{-1}); $\int i \, \mathrm{d}t$ represents the charge taken/delivered by the

battery (in Ah); R_b represents internal resistance of battery (in Ω) and i represents battery current.

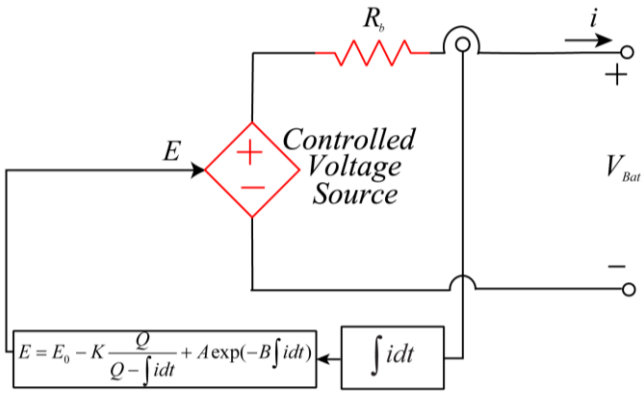

Fig. 6 – *Equivalent circuit diagram of lead-acid battery.*

2.4 Modelling of SC

In this paper, SC model is based on the stern principle that is a combination of Helmholtz model and Gouy Chapman model [22]. Fig. 7 represents an electrical equivalent of SC. The equation for computing SC capacitance can be written as

$$C = \left[\frac{1}{C_{GC}} - \frac{1}{C_H}\right]^{-1}, \tag{11}$$

where

$$C_{GC} = \frac{FQ_C}{2N_e RT}\sinh\left(\frac{Q_C}{N_e^2 A_1\sqrt{8RT\varepsilon\varepsilon_0 C}}\right) \tag{12}$$

and

$$C_H = \frac{N_e A_1 \varepsilon\varepsilon_0}{d} C, \tag{13}$$

where C_{GC} and Q_C are Gouy-chapman capacitance and electric charge of the cell respectively; N_e represents number of electrode layers; R is ideal gas constant, T is absolute temperature; A_1 represents inferential area between electrodes; ε and ε_0 are permitivity of free space and electrolyte material; C is molar concentration; C_H is Helmholtz capacitance and d represents thickness of Helmholtz layer respectively.

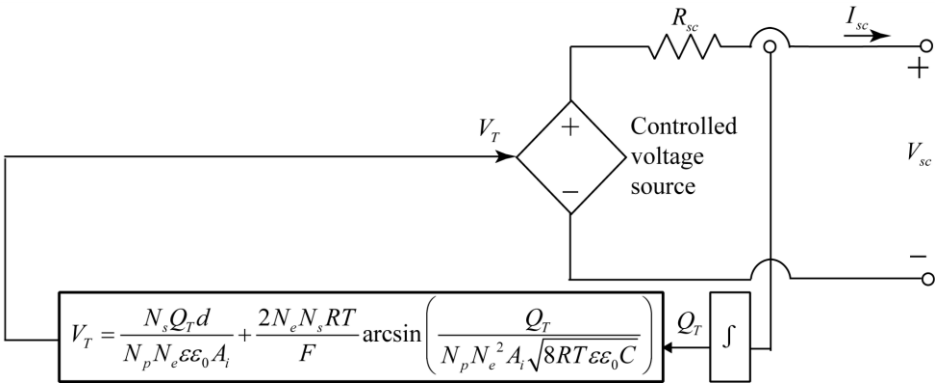

Fig. 7 – *Electrical equivalent of SC.*

To achieve the desired voltage-current ratings, SCs are interconnected in a series-parallel configuration. Total capacitance of SC's stack can be calculated as:

$$C_T = \frac{N_P}{N_S} C \,, \tag{14}$$

here N_S and N_P are number of SCs connected in series and parallel, respectively.

The output voltage of SC stack can be computed as:

$$V_{SC} = \frac{Q_T}{C_T} - R_{SC} I_{SC} \,, \tag{15}$$

where

$$Q_T = N_p Q_C \int I_{SC} \, \mathrm{d}t \,, \tag{16}$$

here Q_T, I_{SC} and R_{SC} represents total charge, total current and total resistance of SC's stack.

3 Proposed Control Strategy

The Block diagram of the proposed control algorithm is shown in Fig. 8. The proposed control strategy aims to enhance the lifetime of battery by reducing stresses on it. An error signal is generated by comparing reference DBV and average actual DBV. Using the error signal as an input, PI controller generates the total reference required for the HESS. The first order low pass filter (LPF) is used to segregate the entire reference current into high-frequency components (I_{HF}^*) and low-frequency components (I_{LF}^*) of reference current signals. The I_{LF}^* can be written as

$$I_{LF}^{*} = f_{LPF}(I_{T}^{*}), \tag{17}$$

where f_{LPF} is function of LPF [22]. A reference current signal for battery has been derived from low-frequency signal I_{LF}^{*} after passing through a rate limiter.

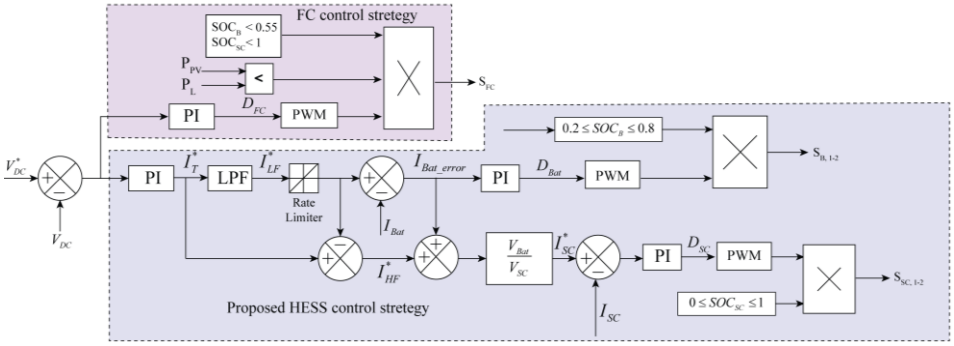

Fig. 8 – *Control strategy for distributing power between FC and HESS.*

The function of the rate limiter is to confine charging/discharging rate of battery. Reference current (I_{Bat}^{*}) of battery can be written as

$$I_{Bat}^{*} = f_{RL}(I_{LF}^{*}), \tag{18}$$

where f_{RL} is the rate limiter function that can be expressed as

$$f_{RL} = \frac{I_{T}^{*}(i) - I_{LF}^{*}(i-1)}{t(i) - t(i-1)}, \tag{19}$$

here $I_{T}^{*}(i)$ and $t(i)$ are current block input and time; $I_{LF}^{*}(i-1)$ and $t(i-1)$ are output and time at the previous step.

The error signal (I_{Bat_error}) is generated by comparing reference (I_{Bat}^{*}) and actual currents of battery (I_{Bat}) and then the error signal is passed through the PI controller to generate duty cycle (D_{Bat}) of PWM generator to obtain switching pulses for BDC converter coupled with battery. High frequency reference current (I_{HF}^{*}) can be written as

$$I_{HF}^{*} = I_{T}^{*} - I_{Bat}^{*}. \tag{20}$$

Battery is unable to track reference current momentarily because of its slow dynamics. Uncompensated battery power can be expressed as

$$P_{Bat\_uncompen} = (I_{HF}^{*} + I_{Bat\_error})V_{Bat}, \tag{21}$$

where V_{Bat} is battery voltage, therefore SC will compensate for uncompensated power of the battery hence reference current of SC can be stated as

$$I_{SC}^{*} = P_{Bat\_uncompen} / V_{SC} = (I_{HF}^{*} + I_{Bat\_error}) V_{Bat} / V_{SC} \ . \tag{22}$$

Actual current of SC is compared with reference current of SC to generate duty cycle for PWM generator, which is connected to BDC associating with SC.

4 PI Controller Design for HESS

BDC switches are triggered in a complementary fashion using a unified controller. An identical transfer function has been used for both buck (charging) and boost (discharging) operating modes of BDC. However, converters are designed primarily based on boost mode of operation. SC has faster dynamics i.e., high charging/discharging rates, and so it is quite an obvious choice for designing parameters of the controllers. The bandwidth of SC's and battery's current control loop (CCL) are limited to 1/6 and 1/10 of switching frequency (f_s) to avoid subharmonics and channelize fast transients towards SC. The bandwidth of converter is kept lower than the right half plane zero frequency (f_{RHPZ}) of SC.

$$f_{RHPZ} = \frac{(1 - D_{SC})R}{2\pi L_{SC}} \ . \tag{23}$$

Because CCL responds faster than voltage control loop (VCL), the voltage control loop's bandwidth is deemed to be smaller than that of CCL.

4.1 Current controller design of SC

The VCL is used to generate reference current for SC. The comparison of reference signal with actual signal generates an error signal for PI controller. Fig. 9, shows block diagram for SC's CCL. The transfer function of CCL is written as [23]

$$G_{id\_SC} = \frac{I_{SC}}{D_{SC}} = \frac{V_{DC} C s + 2\dfrac{V_{DC}}{R}}{L_{SC} C s^2 + \dfrac{L_{SC}}{R} s + (1 - D_{SC})^2} \tag{24}$$

and transfer function of compensator for SC's CCL loop is given as

$$G_{pi\_SC} = K_{p\_SC} + \frac{K_{i\_SC}}{s} \ . \tag{25}$$

The open loop transfer function (OLTF) of CCL is given as

$$G_{ol\_SC} = G_{pi\_SC} G_{id\_SC} H_{SC} \ , \tag{26}$$

here, H_{SC} is current sensor gain.

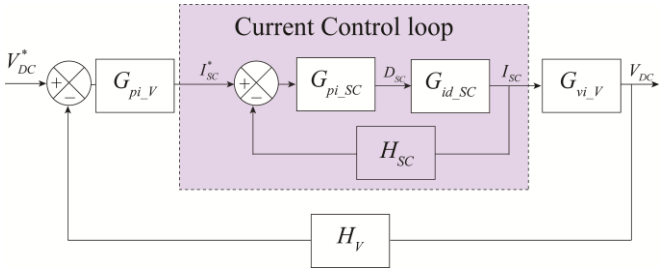

Fig. 9 – *Block diagram of SC current control loop.*

P-I controllers used for proposed work are designed using single input, single output (SISO) toolbox inside Matlab®. The Toolbox aids in the systematic analysis and design of control systems using the transfer function, state-space, zero-pole gain, or frequency response model approaches. Compensators can be fine-tuned to achieve various objectives, including reference tracking, disturbance rejection and stability margins. In this work, Compensators are designed, and the parameters are tuned using a transfer function-based approach to achieve a phase margin (PM) of 60°. The bode plot for uncompensated CCL and compensated CCL are shown in Fig. 10.

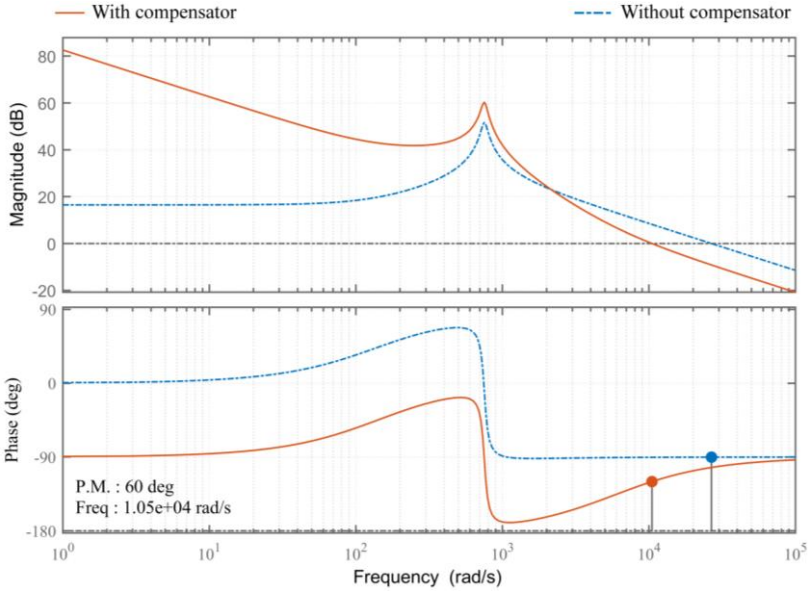

Fig. 10 – *Bode plot of CCL of SC.*

The uncompensated CCL shows the PM of 89.8° at 26.7 krad/s. Systems with more PM are more stable in control system. However, PM of 30-60° is

desirable [24]. Systems with more PM are naturally sluggish and thus unsuitable for the proposed work. So, compensator is designed in a way that PM of loop become 60° at 10.5 krad/s.

4.2 HESS controller design

The transfer function for VCL is expressed as [23]

$$G_{vi\_V} = \frac{V_{DC}}{I_{SC}} = \frac{R(1-D_{SC})\left(1-\left(L_{SC}s\right)/\left(R(1-D_{SC})^2\right)\right)}{2+RCs}. \tag{27}$$

Tranfer function of PI compensator for VCL is given as

$$G_{pi\_V} = K_{p\_V} + K_{i\_V}/s. \tag{28}$$

The OLTF of voltage controller are written as

$$G_{ol\_V} = G_{pi\_V} G_{cl\_SC} G_{vi\_V} H_V \tag{29}$$

and close loop transfer function can be calculated as

$$G_{cl\_SC} = \frac{G_{pi\_SC} G_{id\_SC}}{1+G_{pi\_SC} G_{id\_SC} H_{SC}}. \tag{30}$$

Fig. 11 shows Bode response for both uncompensated and compensated VCL. VCL without compensator shows a PM of 84.3° at 1.54 krad/s. VCL compensator is designed to achieve a PM of 60° at 3.02 krad/s, according to the design criteria.

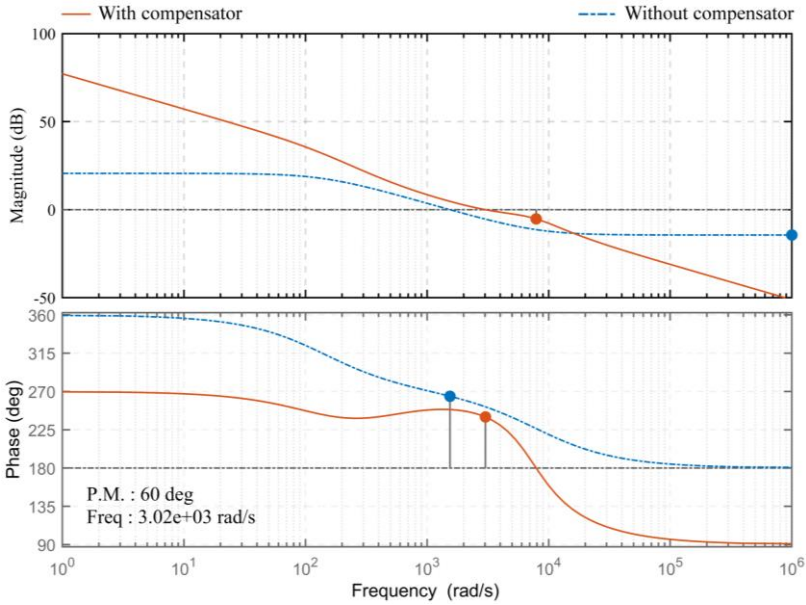

Fig. 11 – *Bode plot of VCL of HESS.*

4.3 Design of battery current controller

Block diagram for the battery current controller loop (BCCL) is shown in Fig. 12. The transfer function of current controller can be written as

$$G_{id\_Bat} = \frac{I_{Bat}}{D_{Bat}} = \frac{V_{DC}Cs + 2\dfrac{V_{DC}}{R}}{L_{Bat}Cs^2 + \dfrac{L_{Bat}}{R}s + (1 - D_{Bat})^2}, \tag{31}$$

transfer function for PI compensator is written as

$$G_{pi\_Bat} = K_{p\_Bat} + K_{i\_Bat}/s \tag{32}$$

and, OLTF of CCL can be given as

$$G_{ol\_Bat} = G_{pi\_Bat}G_{id\_Bat}H_{Bat}. \tag{33}$$

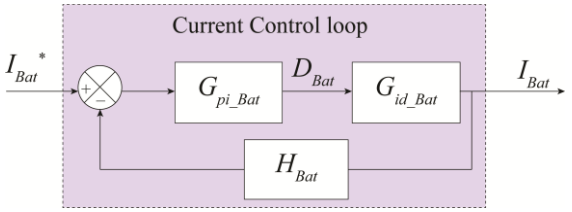

Fig. 12 – *Block diagram of BCCL.*

Bode plot without and with controller for BCCL is shown in Fig. 13.

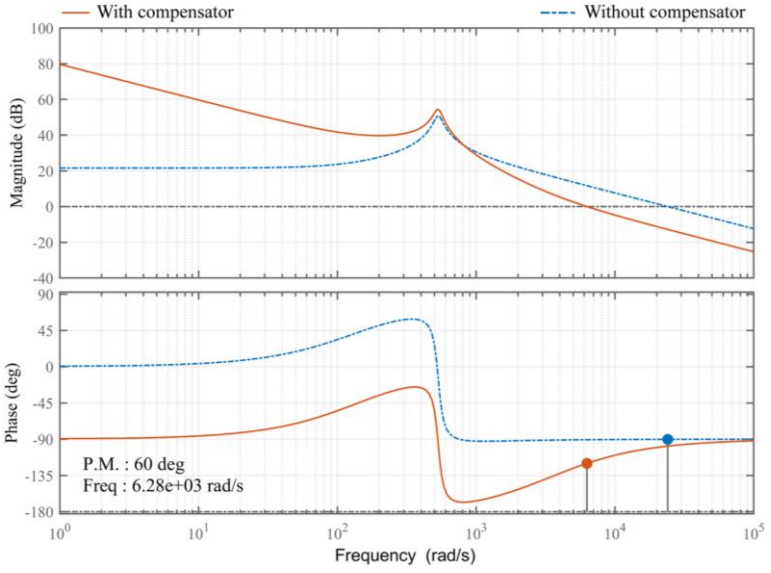

Fig. 13 – *Bode plot of BCCL.*

Uncompensated battery CCL shows a PM of 89.8° at 240.12 krad/s, whereas tuned PI controller achieves the desired PM of 60° at 6.28 krad/s.

5 Result and Discussion

The proposed DCMG shown in Fig. 4 is modelled and simulated using Simscape™ module of MATLAB® software. Parameter matrices for various components used for proposed microgrid are shown in **Table 1**. The effectiveness of the poposed EMS is tested for following two conditions:

– **Case 1:** Variation in the PV generation due to intermittency in solar irrandiance, and
– **Case 2:** Variation in the load demand.

Table 1

Parameter matrices for various components used for proposed microgrid. (Part I)

PV Array	***Nos./Values***
Cells per module	72
Open circuit Voltage (V_{oc})	21 V
Parallel strings	1
Series connected modules per string	2
Short circuit current (I_{SC})	8 A
FC Specifications	
FC type	*PEMFC*
Stack power	
Maximal	2000 W
Nominal	1259.96 W
FC resistance	0.061871 Ω
Nernst voltage of one cell	1.115 V
Nominal Utilization	
Hydrogen	99.92 %
Oxidant	1.813 %
Nominal Consumption	
Fuel	15.22 slpm
Air	36.22 slpm
Fuel flow rate at nominal hydrogen utilization	
Maximum	23.46 lpm
Nominal	12.2 lpm
Air flow rate at nominal oxidant utilization	
Maximum	4615 lpm
Nominal	2400 lpm
Air supply pressure	1 bar
Fuel supply pressure	1.5 bar
System temperature	328 K

Table 1
Parameter matrices for various components used for proposed microgrid. (Part II)

Battery Specifications	***Nos./Values***
Type	*Lithium-Ion*
Nominal voltage	24 V
Rated capacity	14 Ah
SC specifications	
Equivalent DC series resistance	0.003 Ω
Rated capacitance	29 F
Rated Voltage	32 V
DC-DC Converters	
L_{SC}	1.8 mH
L_{PV}	10 mH
L_{Bat}	2 mH
C_{DC}	440 µF
Switching frequency (f_s)	10 kHz
Nominal load resistance (R)	32 Ω
Compensators Parameters	
K_{p_SC}	0.34
K_{i_SC}	2021
K_{p_V}	1.61
K_{i_V}	674
K_{p_Bat}	0.23
K_{i_Bat}	8000

5.1 Simulation results

5.1.1 Case 1: Variation in PV generation

In this case, consistensy of the proposed system is tested for variation in PV generation. From Fig. 14b, in $T_1 – T_2$ and $T_7 – T_8$ intervals PV generates power according to solar irradiance of 600 W/m^2 and 650 W/m^2 as shown in Fig. 15b, which is more than demand power required by load, i.e. system is working in surplus power mode (SPM). From Fig. 14c, it is clear battery absorbs this surplus power by charging, while high-frequency transients are absorbed by SC. FC remains in an idle state as PV generates surplus power.

In the interval $T_2 – T_7$, PV operates in deficit power mode (DPM) as power generated by the PV is less than the power required by the load as shown in Fig. 14b. FC and battery provide power and mitigate disparity in power. The FC

generation is controlled in such a way that it minimizes stresses on battery. SC reduces battery stress by compensating for high-frequency transients.

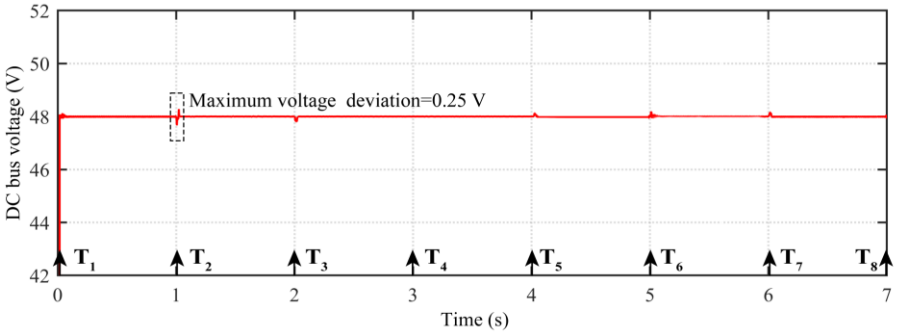

(a)

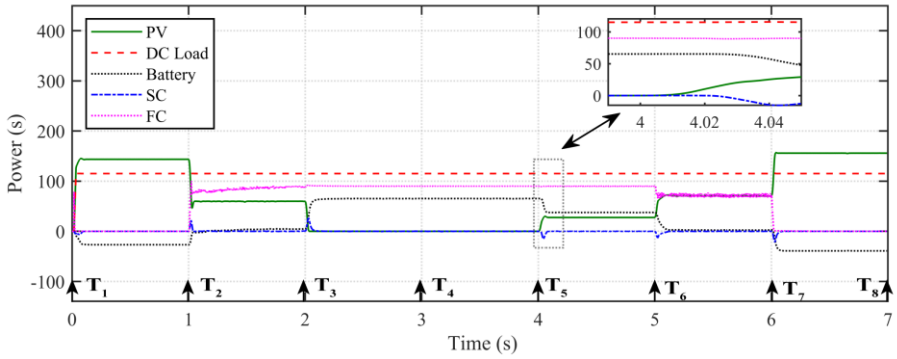

(b)

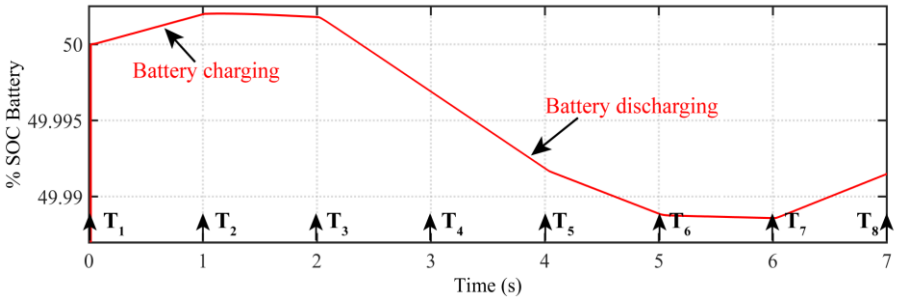

(c)

Fig. 14 – *Simulation results for Case 1:* (a) *DC bus voltage;* (b) *Power sharing;* (c) *SOC variation of the battery.*

SOC variation for battery and SC has been shown in Figs. 14c and 15a. From the Fig. 14a it is clear that the maximum deviation is 0.25 V, which satisfies

criterion of IEEE standards prescribing the maximum 5% deviation in the DBV. Fig. 15b, shows the time variation in solar irradiance.

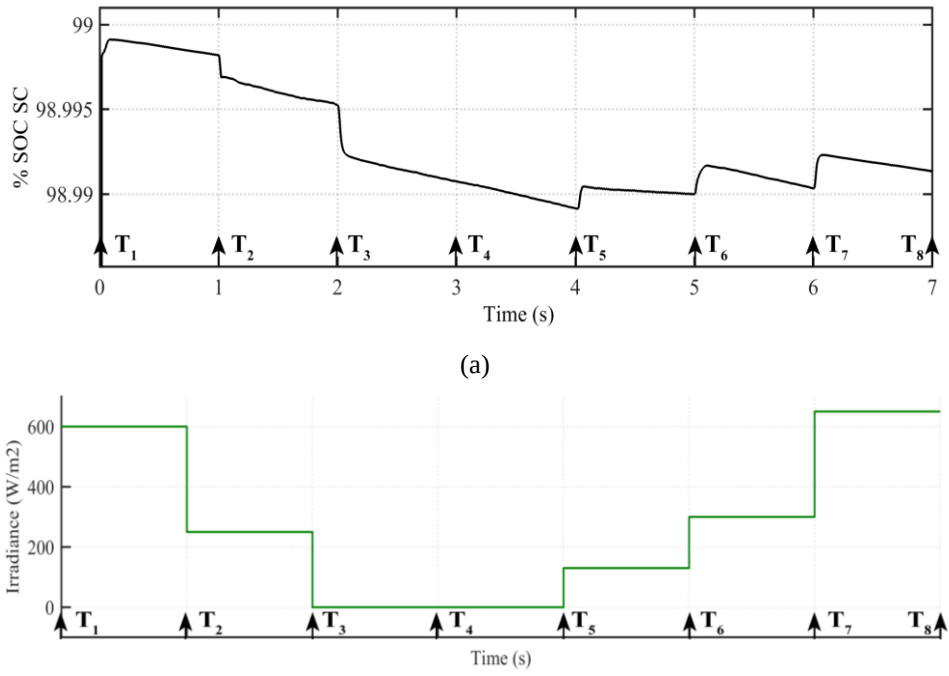

Fig. 15 – *Simulation results for Case 1:*
(a) *SOC variation of SC;* (b) *Variation in solar irradiance.*

5.1.2 Case 2: Change in Load demand

Fig. 16b shows system constraits for variation in load demand. Interval T_3 to T_6 depicts DPM, i.e., the condition when load demand exceeds PV power generation. From Figs. 16b and 16c, it can be inferred that battery SOC is lower than 0.55, as a result battery and FC supply power to maintain a balance between generation and load demand. FC provides power when load demand exceeds PV generation and battery SOC is less than 0.55. SC supplies power only during the sudden variation in load and hence reducing stresses on the battery. As shown in Fig. 16b, PV generates surplus power in intervals $T_1 - T_3$ and $T_6 - T_8$. As a result, battery charges and stores energy that can be utilised when load demand exeeds PV generation. DBV is maintained throughout the operation at its reference value and maximum deviation is 0.51 V as shown in Fig. 16a, which falls under ±5% criterion as prescribed by IEEE.

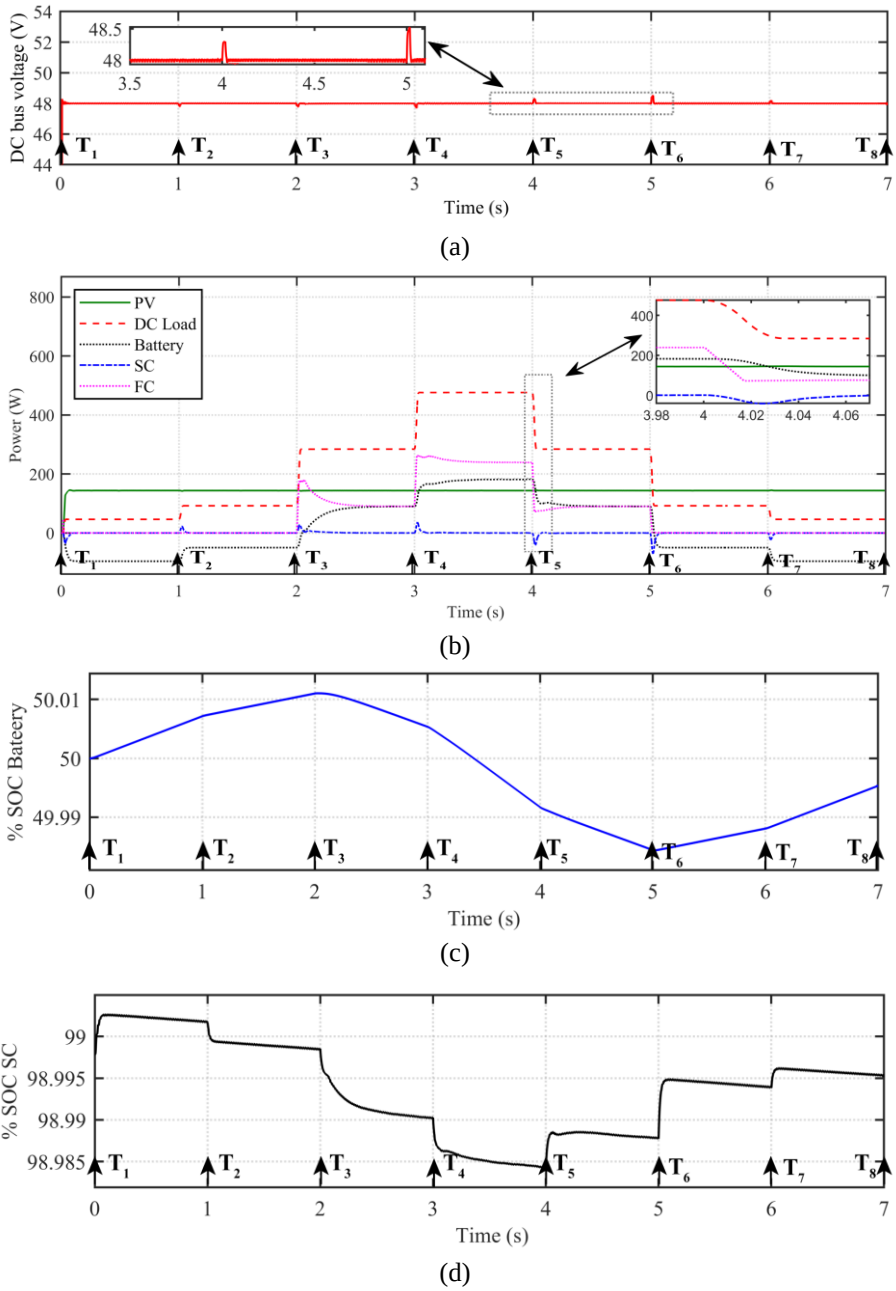

Fig. 16 – *Simulation results for Case 2:* (a) *DC bus voltage;* (b) *Power sharing among various units;* (c) *SOC variation of battery;* (d) *SOC variation of SC.*

5.2 Experimental results

The proposed prototype model of the microgrid incorporating PV, FC, DC load, battery and SC is simulated and then verified using an experimental setup as shown in Fig. 17. Experimental setup consists of a high-end reconfigurable FPGA-based real-time simulator Opal-RT (OP 5700), a host PC, UPS, and a four-channel digital mixed signal oscilloscope (MSO). Figs. 18a, 18b and 18c represent Case 1, while Figs. 19a, 19b, and 19c represent Case 2.

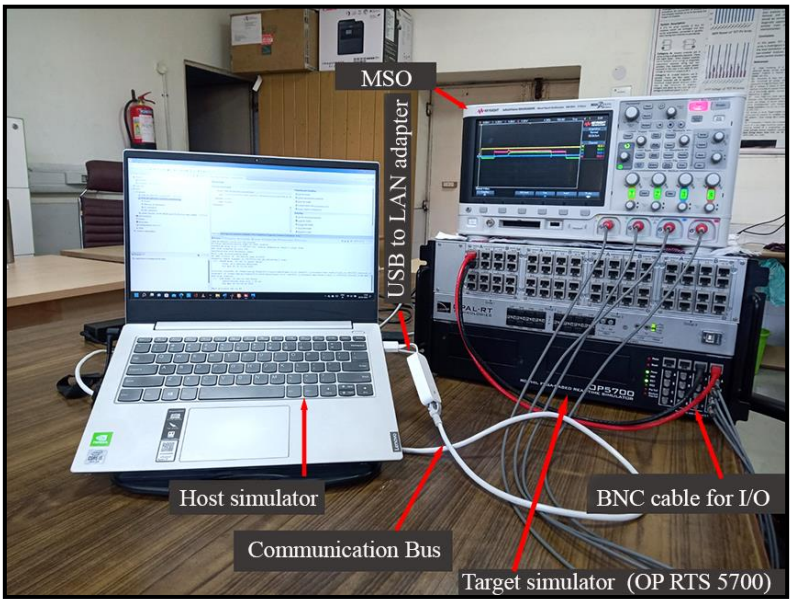

Fig. 17 – *Experimental setup with FPGA based real time simulator (OPAL-RT).*

5.2.1 Case 1: Variation in PV generation

Fig. 18c depicts stepped change in PV power generation that is in accordance with solar irradiance. From Figs. 18b and 18c, in intervals $T_1 - T_2$ and $T_7 - T_8$ load demands are less than power PV power generation. Fig. 18b displays battery storing extra power by charging when FC do not produce any power. In $T_2 - T_7$, load demand is more than PV power generation, can be observed in Figs. 18b and18c. As a result, battery discharges and FC also generate power as battery SOC is less than 0.55. HESS controller diverts high frequency transients towards SC and low frequency transients towards battery and hence reducing dynamic stresses on battery which results in increased battery life time.

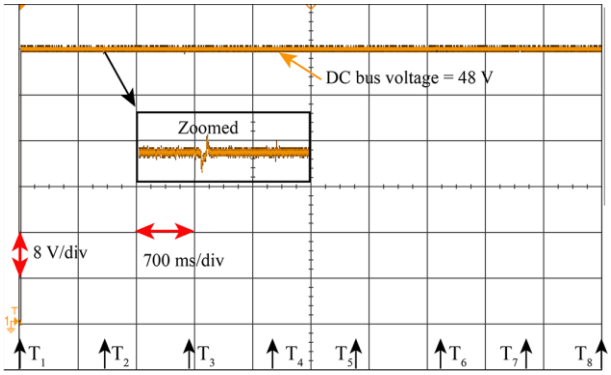

(a)

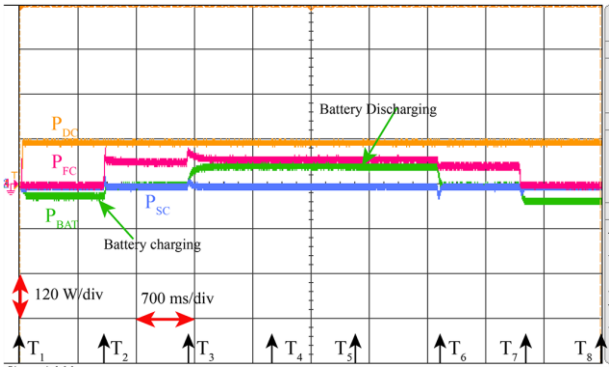

(b)

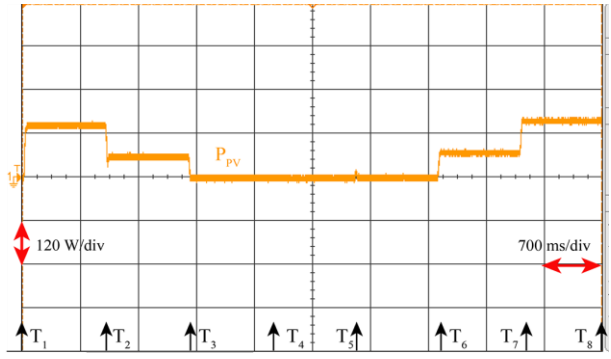

(c)

Fig. 18 – *Experimental results for Case 1;* (a) *DC bus voltage;* (b) *Power sharing among DC load, FC, and batter;* (c) *Power sharing by PV.*

5.2.2 Case 2: Change in Load demand

Fig. 19b shows change in load demand.

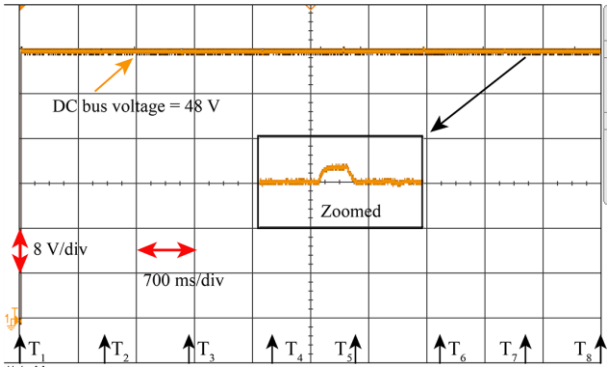

(a)

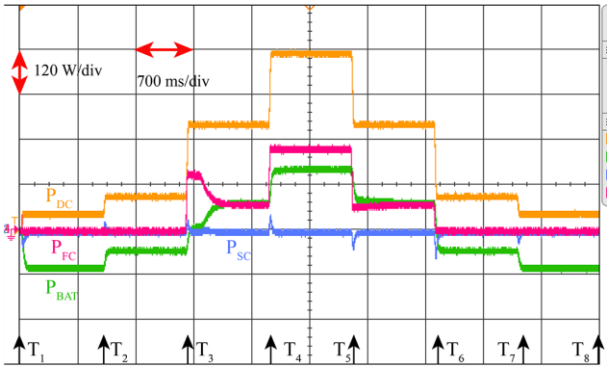

(b)

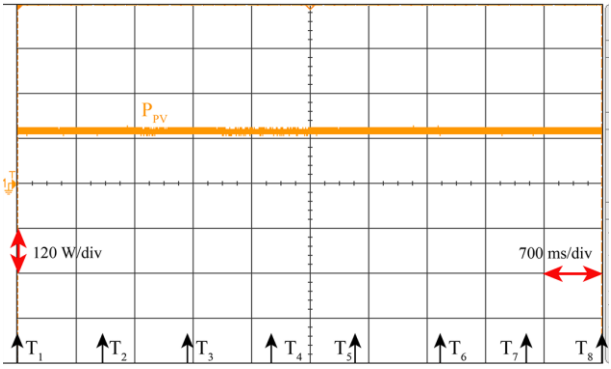

(c)

Fig. 19 – *Experimental results for Case 1:* (a) *DC bus voltage;* (b) *Power sharing among DC load, FC, and batter;* (c) *Power sharing by PV.*

Figs. 19b and 19c indicate in T_3 to T_6, load power demands are higher than PV power generation. Imbalance in PV generation and load demand is met using battery discharging and FC generation. From Figs.19b and 19c in intervals $T_1 - T_3$ and $T_6 - T_8$, DC load demand is less than PV generation. Hence battery utilizes excess power and stores it for further utilization, while FC remains in standby mode. HESS controller diverts high frequency variation in load demands to SC. SC reduces stresses on battery and thus results in its increased life-time.

In both the Case 1 and in Case 2 DBV is maintained at reference value irrespective variation in solar irradiance and load. The maximum deviation is 0.51 V that is less than 5% and hence follows the IEEE standards.

6 Conclusion

A novel control technique with EMS is proposed for a DCMG with HESS to effectively regulate the DBV regardless of the fluctuations in demand-generation and increase battery life through reduced stress. The proposed controller for DBV regulation is designed for good transient response, and stability analysis of HESS is ascertained. The proposed control strategy directs the rapid fluctuation in power demand along with uncompensated battery components towards SC. In addition to better DBV regulation, the proposed strategy admits a significant reduction in the charge/discharge rate of the battery, resulting in improved battery life. Further, the proposed controller and EMS maintains SOC under the desired limit. The proposed control strategy is simulated, and the efficacy of the proposed DCMG is further validated using a real-time simulator opal-RT (OP-5700) for variations in demand and generation.

7 References

[1] M. Srinivasan, A. Kwasinski: Control Analysis of Parallel DC-DC Converters in a DC Microgrid with Constant Power Loads, International Journal of Electrical Power & Energy Systems, Vol. 122, November 2020, p. 106207.

[2] A. Jhunjhunwala, P. Kaur: Solar Energy, DC Distribution, and Microgrids: Ensuring Quality Power in Rural India, IEEE Electrification Magazine, Vol. 6, No. 4, December 2018, pp. 32 – 39.

[3] A. M. Gee, F. V. P. Robinson, R. W. Dunn: Analysis of Battery Lifetime Extension in a Small-Scale Wind-Energy System Using Supercapacitors, IEEE Transactions on Energy Conversion, Vol. 28, No. 1, March 2013, pp. 24 – 33.

[4] A. Q. Almousawi, A. A. Aldair: A New Energy Management Control Strategy for PV-Battery Hybrid System, International Journal of Computing and Digital Systems, Vol. 12, No. 1, July 2022, pp. 427 – 437.

[5] I. Serban, C. Marinescu: Battery Energy Storage System for Frequency Support in Microgrids and with Enhanced Control Features for Uninterruptible Supply of Local Loads, International Journal of Electrical Power & Energy Systems, Vol. 54, January 2014, pp. 432 – 441.

[6] Z. Yi, W. Dong, A. H. Etemadi: A Unified Control and Power Management Scheme for PV-Battery-Based Hybrid Microgrids for Both Grid-Connected and Islanded Modes, IEEE Transactions on Smart Grid, Vol. 9, No. 6, November 2018, pp. 5975 – 5985.

[7] M. Ding, B. Wang, Zh. Chen, Z. Chen, Y. Luo, G. Zheng: Stabilizing Control Strategy of Complementary Energy Storage in Renewable Energy System, Proceedings of the IEEE PES Innovative Smart Grid Technologies, Tianjin, China, May 2012, pp. 1 – 5.

[8] M. H. Saeed, W. Fangzong, B. A. Kalwar, S. Iqbal: A Review on Microgrids' Challenges & Perspectives, IEEE Access, Vol. 9, 2021, pp. 166502 – 166517.

[9] Z. Cabrane, J. Kim, K. Yoo, M. Ouassaid: HESS-Based Photovoltaic/Batteries/ Supercapacitors: Energy Management Strategy and DC Bus Voltage Stabilization, Solar Energy, Vol. 216, March 2021, pp. 551 – 563.

[10] M. D. Lukas, K. Y. Lee, H. Ghezel-Ayagh: Development of a Stack Simulation Model for Control Study on Direct Reforming Molten Carbonate Fuel Cell Power Plant, IEEE Transactions on Energy Conversion, Vol. 14, No. 4, December 1999, pp. 1651 – 1657.

[11] M. D. Lukas, K. Y. Lee, H. Ghezel-Ayagh: Modeling and Cycling Control of Carbonate Fuel Cell Power Plants, Control Engineering Practice, Vol. 10, No. 2, February 2002, pp. 197 – 206.

[12] S. Obara: Analysis of a Fuel Cell Micro-Grid with a Small-Scale Wind Turbine Generator, International Journal of Hydrogen Energy, Vol. 32, No. 3, March 2007, pp. 323 – 336.

[13] M. Patterson, N. F. Macia, A. M. Kannan: Hybrid Microgrid Model based on Solar Photovoltaic Battery Fuel Cell System for Intermittent Load Applications, IEEE Transactions on Energy Conversion, Vol. 30, No. 1, March 2015, pp. 359 – 366.

[14] B. Dong, Y. Li, Z. Zheng, L. Xu: Control Strategies of Microgrid with Hybrid DC and AC Buses, Proceedings of the 14th European Conference on Power Electronics and Applications, Birmingham, UK, August 2011, pp. 1 – 8.

[15] B. Dong, Y. Li, Z. Zheng: Composite Converter of Hybrid Storage in Distributed Renewable Energy Generation System, Proceedings of the International Conference on Electrical Machines and Systems, Beijing, China, August 2011, pp. 1 – 4.

[16] K. D. Hoang, H.- H. Lee: Accurate Power Sharing with Balanced Battery State of Charge in Distributed DC Microgrid, IEEE Transactions on Industrial Electronics, Vol. 66, No. 3, March 2019, pp. 1883 – 1893.

[17] X. Feng, H. B. Gooi, S. X. Chen: Hybrid Energy Storage with Multimode Fuzzy Power Allocator for PV Systems, IEEE Transactions on Sustainable Energy, Vol. 5, No. 2, April 2014, pp. 389 – 397.

[18] B. Hredzak, V. G. Agelidis, M. Jang: A Model Predictive Control System for a Hybrid Battery-Ultracapacitor Power Source, IEEE Transactions on Power Electronics, Vol. 29, No. 3, March 2014, pp. 1469 – 1479.

[19] F. Akar, Y. Tavlasoglu, B. Vural: An Energy Management Strategy for a Concept Battery/Ultracapacitor Electric Vehicle with Improved Battery Life, IEEE Transactions on Transportation Electrification, Vol. 3, No. 1, March 2017, pp. 191 – 200.

[20] A. A. Kamel, H. Rezk, N. Shehata, J. Thomas: Energy Management of a DC Microgrid Composed of Photovoltaic/Fuel Cell/Battery/Supercapacitor Systems, Batteries, Vol. 5, No. 3, September 2019, p. 63.

[21] M. Y. El-Sharkh, A. Rahman, M. S. Alam, P. C. Byrne, A. A. Sakla, T. Thomas: A Dynamic Model for a Stand-Alone PEM Fuel Cell Power Plant for Residential Applications, Journal of Power Sources, Vol. 138, No. 1-2, November 2004, pp. 199 – 204.

[22] K. B. Oldham: A Gouy–Chapman–Stern model of the double layer at a (metal)/(ionic liquid) interface, Journal of Electroanalytical Chemistry, Vol. 613, No. 2, February 2008, pp. 131 – 138.

[23] Y. Jin, J. Xu, G. Zhou, Ch. Mi: Small-Signal Modeling and Analysis of Improved Digital Peak Current Control of Boost Converter, Proceedings of the IEEE 6th International Power Electronics and Motion Control Conference, Wuhan, China, May 2009, pp. 326 – 330.

[24] S.- H. Kim: Electric Motor Control: DC, AC, and BLDC Motors, 1st Edition, Elsevier Science, Amsterdam, 2017.